Supplemental Materials

Molecular Biology of the Cell

Mbom et al.

Supplemental Table 1:
Nek2 phosphorylation of β-catenin identified on residues 23, 29, 33, 102, 556, 675 and within 37-42 by nano-LC-MS/MS. (A) Phospho-peptide enumeration and sequence of beta-catenin phosphorylation by Nek2. (B) Control sample used was beta-catenin incubated with Nek2 in the absence of ATP. Phosphopeptides identified in the control sample were excluded.

Supplemental Figure 1.
Nek2 phosphorylation of β-catenin identified by nano-LC-MS/MS. (A) Fragmentation patterns of the +4 charged ion 812.113, identifying phosphorylation at sites 23, and 29 from the β-catenin peptide digests. The amino acid sequence of the peptide fragment is shown with the phosphorylation site labeled as pS or pT within each spectrum with the b and y ions labeled. (B) Fragmentation pattern from two scans for the +4 charged ion 792.121 and +5 charged ion 633.898, identifying a phosphorylation site at position 33. (C) Fragmentation pattern of the +4 charged ion 812.113 with phosphorylation site at 33, and another phosphorylation site within residues 37-42. (D) The fragmentation pattern from the +4 charged ion 821.3692 with phosphorylation site at position 102. (E) Fragmentation pattern from two scans, including the doubly charged ion 852.874 and triply charged ion 568.919 with phosphorylation site at position 556. (F) The fragmentation pattern from the triply charged ion 523.246 with phosphorylation site at position 675. The residue at position 679 was also identified in the control (Nek2 incubation without ATP), and therefore excluded as a Nek2 phosphorylation site.

Supplemental Figure 2. (A). HEK293 cells were transfected as indicated. Cell lysates extracted with NP40 were immunoprecipitated with GFP-antibody and half of each sample was treated with the deubiquitinating enzyme, Usp2 for 30 minutes at 37°C. Immunoprecipitates were immunoblotted with antibodies specific for HA and GFP.

Supplemental Figure 3. (A) The refractive indices of sucrose gradient fractions from the mitotic and asynchronous centrosome enrichment were graphed against the percentage of sucrose in the gradient. (B) The refractive index of each fraction from mitotic and asynchronous centrosome enrichments. (C) Centrosome-positive (13/14) and centrosome-negative (21/22) fractions from the sucrose gradients of mitotic and asynchronus cell extracts were pooled and immunoprecipitated with the phospho-S33/S37/T41 antibody, and then immunoblotted for phospho-S33/S37/T41 proteins. The western blot is a high intensity scan of the blot shown in Figure 3E showing an additional high molecular weight proteins (*) precipitating with the phospho-S33/S37/T41 antibody from the centrosome-positive mitotic fraction.

Supplemental Figure 4. Activity of GSK3 inhibitors on MG132-stabilized phospho-β-catenin. (A) HCT116 lines expressing either wild type β-catenin and ΔS45 β-catenin (Par$^{WT/\Delta S45}$), or only ΔS45 β-catenin (18$^{-/\Delta S45}$) were treated for 4 hours with 0.2% DMSO as a control or with 25 μM MG132 with or without the following GSK3 inhibitors: 20 μM SB216763 (SB), 5 μM GSK3 inhibitor IX (IX), 20 mM LiCl. Following extraction with SDS, equal amounts of protein were separated by SDS-PAGE and immunoblotted with antibodies to β-catenin (red) and phospho-S33/S37/T41 β-catenin (green). MG132-

treatment increases phospho-S33/S37/T41 β-catenin (p-β-cat. in green) over total β-catenin (β-cat. in red) only in parental cells expressing wild-type β-catenin (compare lane 1, 2) but not in HCT116 $18^{-/\Delta S45}$ cells expressing β-catenin without the CK1 priming site S45 for GSK3 phosphorylation (compare lane 6, 7). MG132-induced increase in phopsho-S33/S37/T41 β-catenin is inhibited efficiently by co-treatment with GSK3 inhibitors SB216763 (SB) or IX, and less efficiently by 20 mM LiCl (lanes 3 to 5). (B, C) HCT116 $18^{-/\Delta S45}$ cells (B) and HCT116 $85^{WT/-}$ cells (C) were treated with 2% DMSO as a control or with different GSK3 inhibitors (20µM SB21673, 5µM GSK3 Inhibitor IX or 20mM LiCl) for 4 hours and then processed for immunofluorescence of mitotic spindles with antibodies as indicated and co-stained with DAPI for DNA (blue in merge). For presentation of control spindles and different treatments, images were taken at identical exposure times and identically contrast-enhanced for each stain. Scale bar: 5 µm. Quantitations of phospho-S33/S37/T41 reactivity at spindle poles are shown in Figure 4E.

Supplemental Table 1

A Beta-catenin incubated with Nek-2 and ATP

Peptide	Sequence	Phosphosite
20-49	AAVSHWQQQSYLDSGIHSGATTTAPSLSGK	S23, S29, S33, 37-42
96-124	AAMFPETLDEGMQIPSTQFDAAHPTNVQR	T102
551-565	TSMGGTQQQFVEGVR	T556
673-684	RLSVELTSSSLFR	S675

B Beta-catenin control sample incubated with Nek-2 without ATP

Peptide	Sequence	Phosphosite
551-565	TSMGGTQQQFVEGVR	S552
673-684	RLSVELTSSSLFR	T679, S681

Supplemental Figure 1

(A) 23, 29

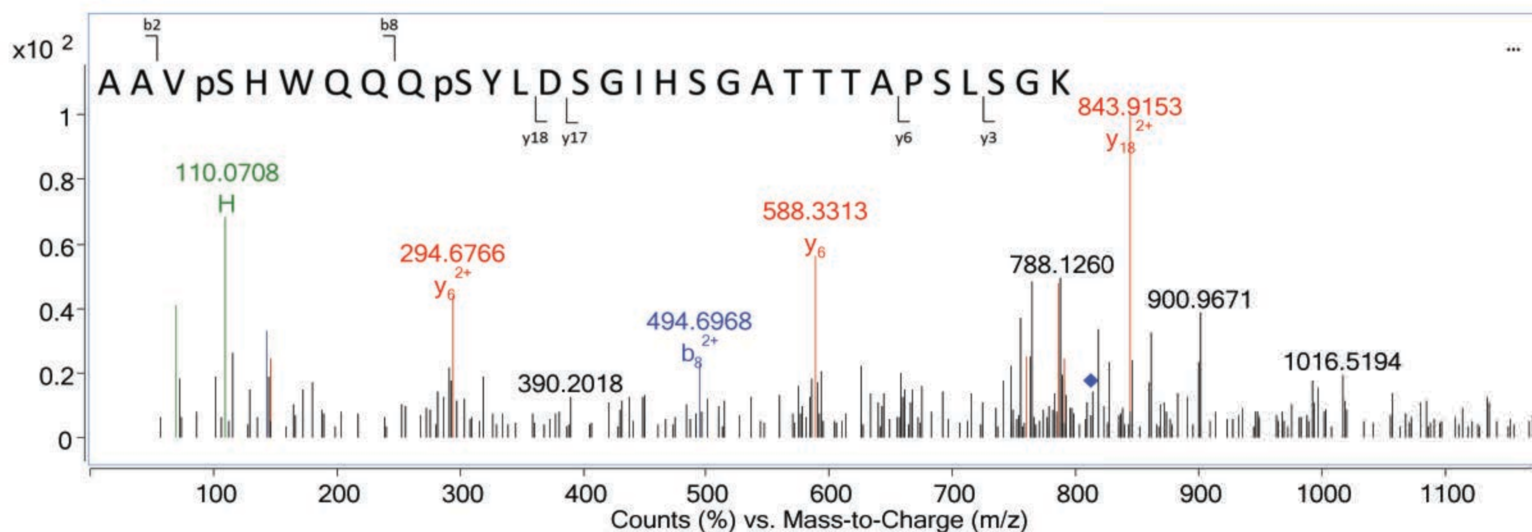

(B) 33

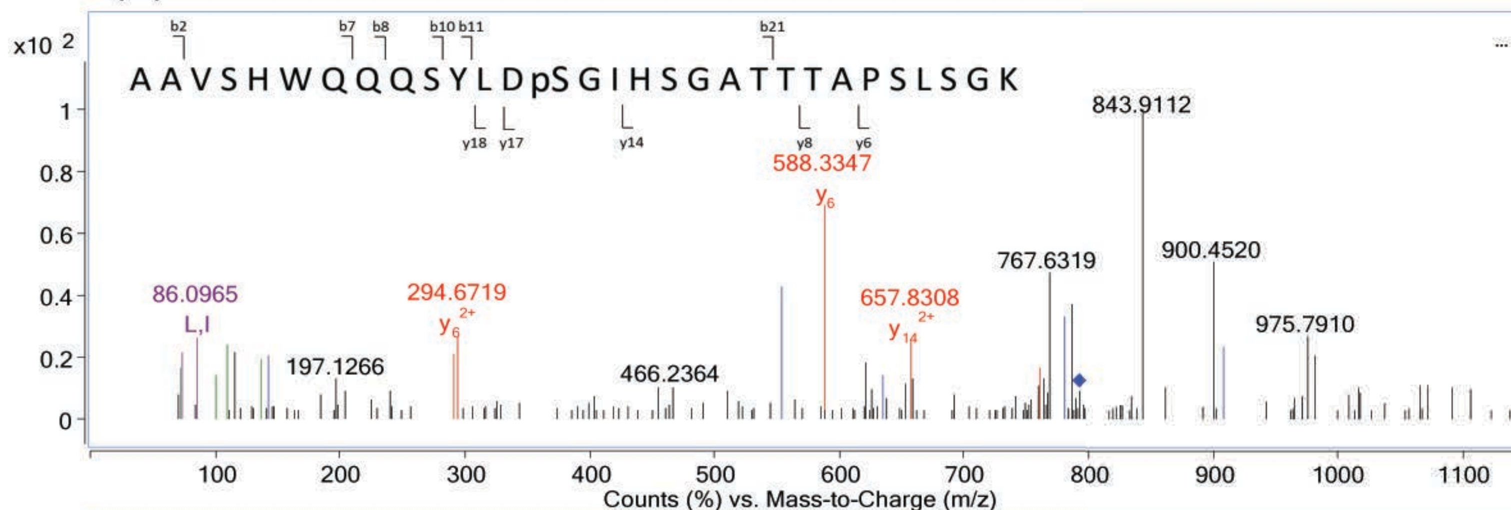

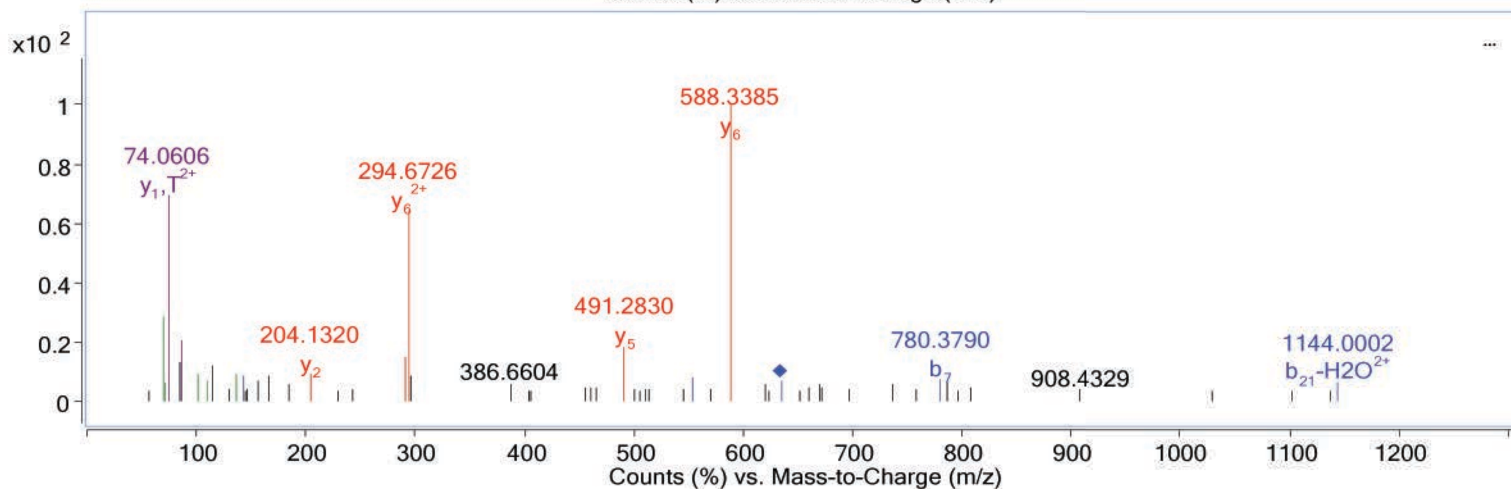

Supplemental Figure 1

(C) 37-42

x10 2

b7 B10-H20

A A V S H W Q Q Q S pY L P D S G I H p(S G A T T T) A P S L S G K

y18 y6

588.3312 y_6

883.9051 y_{18}^{2+}

780.3782 b_7

668.2940

115.0843

291.1664

454.7192

940.9626

1056.4718

Counts (%) vs. Mass-to-Charge (m/z)

(D) 102

x10 2

b3 b4

A A M F P E pT L D E G M Q I P S T Q F D A A H P T N V Q R

y16 y15 y14 y9 y6

834.9076 y_{15}^{2+}

86.0971 L,I

556.9381 y_{15}^{3+}

714.3931 y_6

274.1200 b_3

421.1845 b_4

891.4481 y_{16}^{2+}

1108.5319 y_{10}

157.0981

Counts (%) vs. Mass-to-Charge (m/z)

Supplemental Figure 1

(E) 556

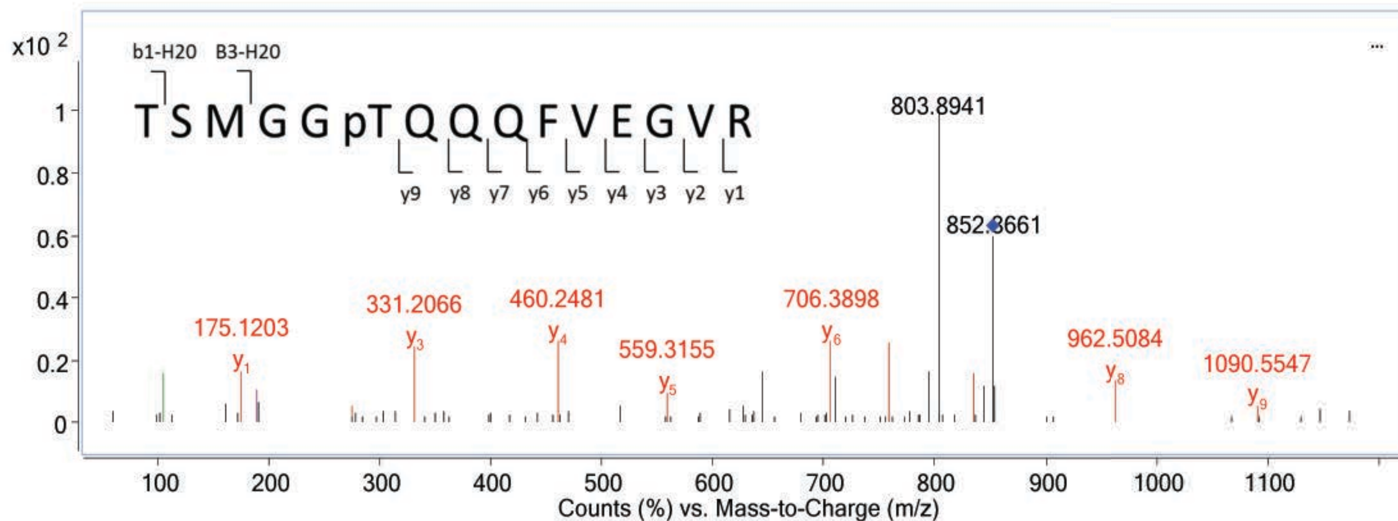

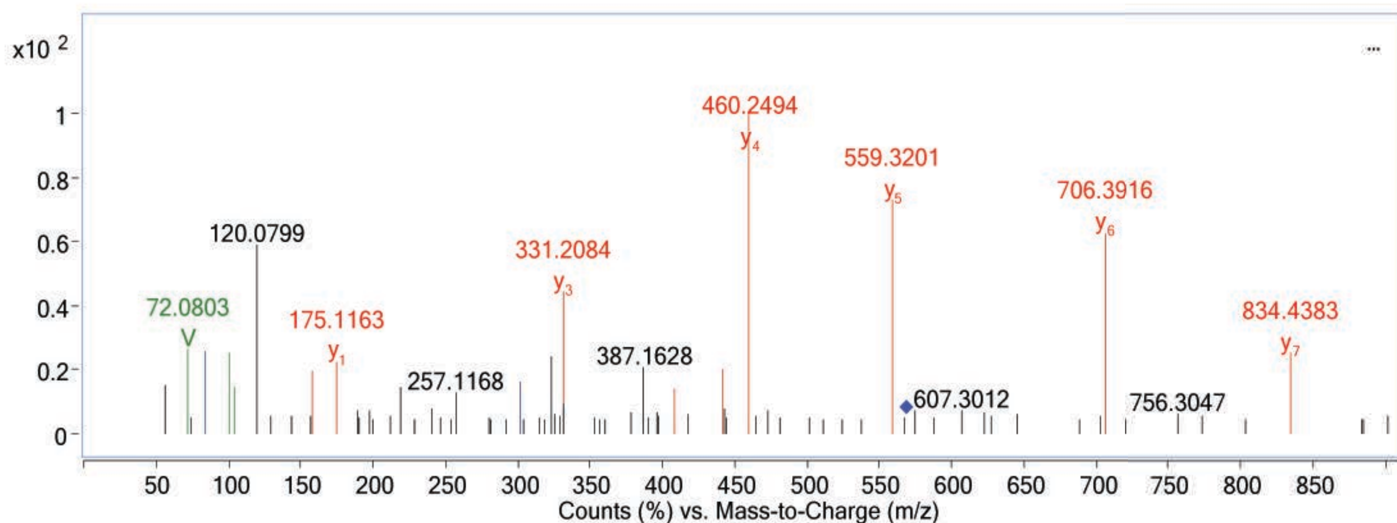

(F) 675

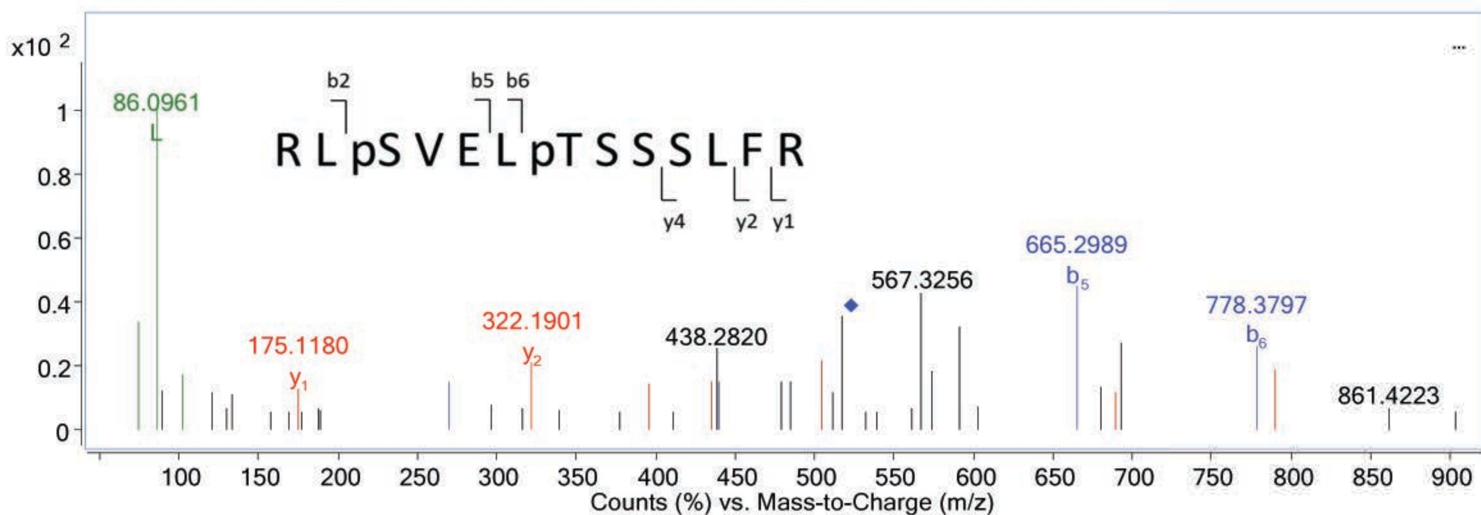

Supplemental Figure 2

A

GFP-β-catenin	+	+	+	+	+	+
HA-Ubiquitin	+	+	+	+	+	+
Nek2	-	-	+	+	-	-
KD-Nek2	-	-	-	-	+	+
deUB enzyme	-	+	-	+	-	+

IB: HA

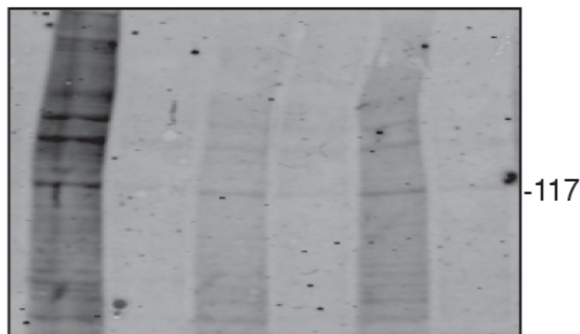

IB: GFP

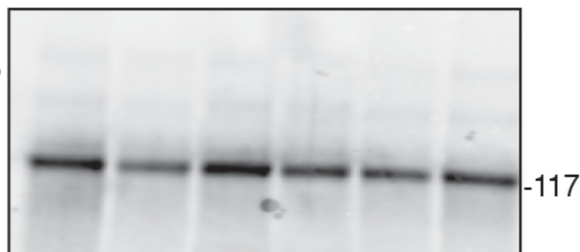

Supplemental Figure 3

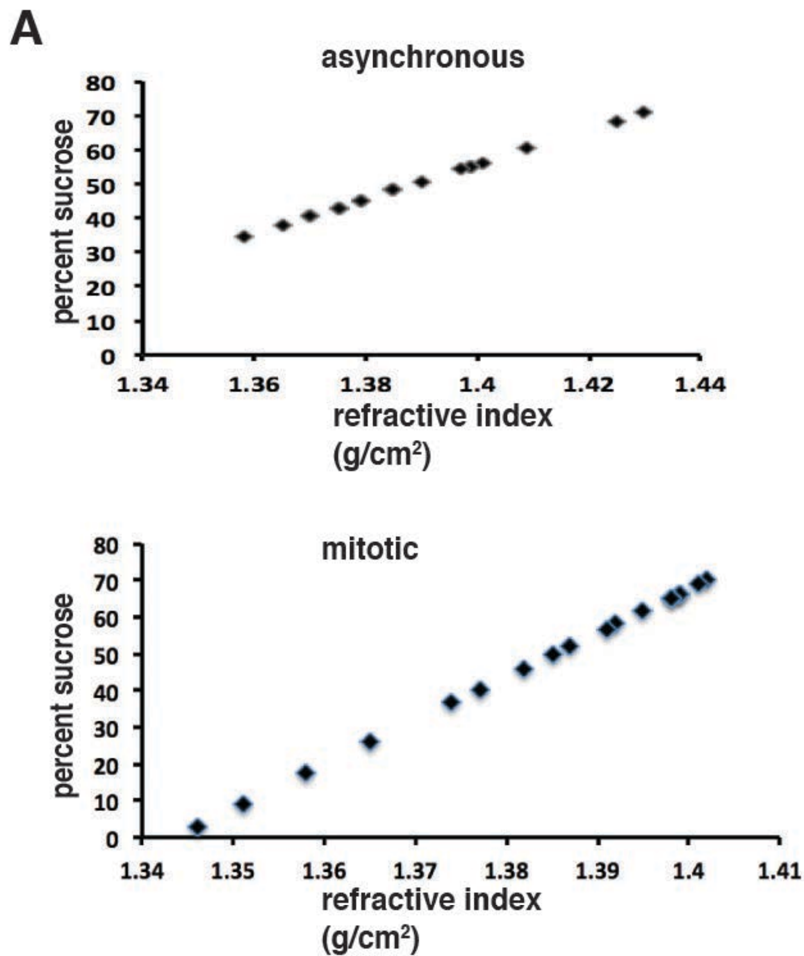

B

mitotic		asynchronous	
fraction number	refractive index	fraction number	refractive index
1	1.402	1	1.430
2	1.401	2	1.425
3	1.399	3	1.409
4	1.399	4	1.401
5	1.398	5	1.399
6	1.398	6	1.399
7	1.395	7	1.397
8	1.392	8	1.390
9	1.391	9	1.385
10	1.387	10	1.385
11	1.385	11	1.379
12	1.382	12	1.379
13	1.377	13	1.375
14	1.374	14	1.375
15	1.365	15	1.370
16	1.358	16	1.370
17	1.351	17	1.365
18	1.346	18	1.358

C

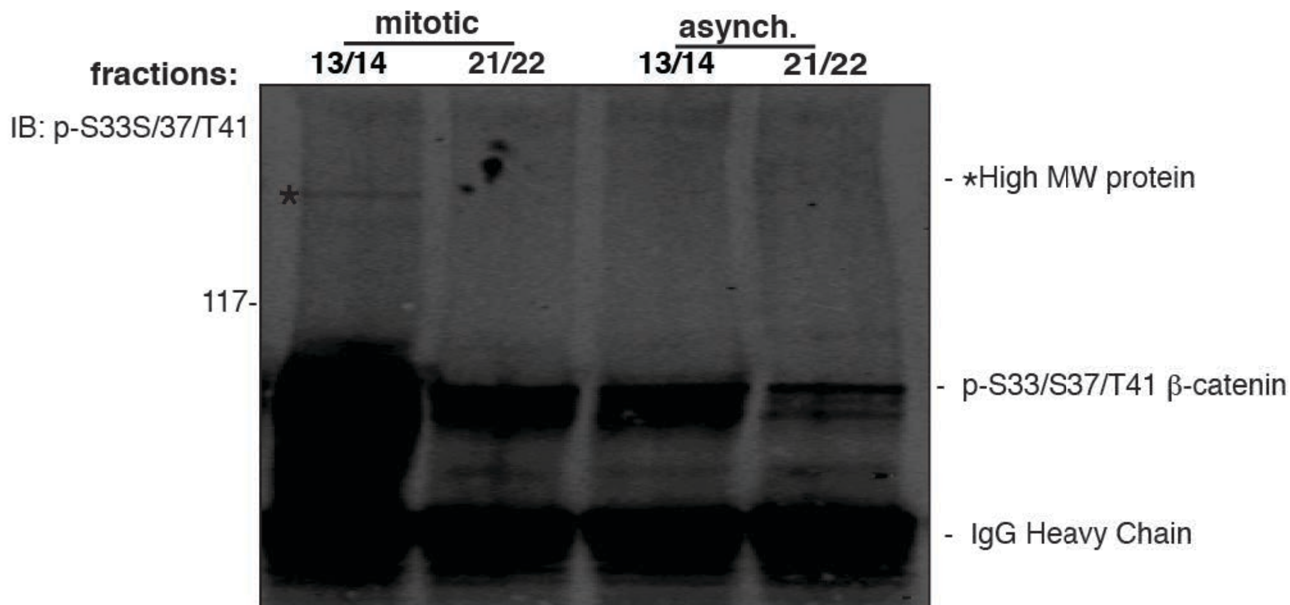

Supplemental Figure 4